⌘ *Author's Choice*

THE JOURNAL OF BIOLOGICAL CHEMISTRY VOL. 285, NO. 43, pp. 33324–33337, October 22, 2010

Control of Activating Transcription Factor 4 (ATF4) Persistence by Multisite Phosphorylation Impacts Cell Cycle Progression and Neurogenesis*[S]

Received for publication, May 3, 2010, and in revised form, July 19, 2010 Published, JBC Papers in Press, August 19, 2010, DOI 10.1074/jbc.M110.140699

Christopher L. Frank[‡], Xuecai Ge[‡1], Zhigang Xie[‡§1], Ying Zhou[‡], and Li-Huei Tsai[‡¶2]

From the [‡]Massachusetts Institute of Technology, Picower Institute for Learning and Memory, the Howard Hughes Medical Institute, Cambridge, Massachusetts 02139, the Stanley Center for Psychiatric Research, [¶]Broad Institute of Harvard and Massachusetts Institute of Technology, Cambridge, Massachusetts 02139, and the [§]Departments of Neurosurgery and Pharmacology and Experimental Therapeutics, Boston University School of Medicine, Boston, Massachusetts 02118

Organogenesis is a highly integrated process with a fundamental requirement for precise cell cycle control. Mechanistically, the cell cycle is composed of transitions and thresholds that are controlled by coordinated post-translational modifications. In this study, we describe a novel mechanism controlling the persistence of the transcription factor ATF4 by multisite phosphorylation. Proline-directed phosphorylation acted additively to regulate multiple aspects of ATF4 degradation. Stabilized ATF4 mutants exhibit decreased β-TrCP degron phosphorylation, β-TrCP interaction, and ubiquitination, as well as elicit early G_1 arrest. Expression of stabilized ATF4 also had significant consequences in the developing neocortex. Mutant ATF4 expressing cells exhibited positioning and differentiation defects that were attributed to early G_1 arrest, suggesting that neurogenesis is sensitive to ATF4 dosage. We propose that precise regulation of the ATF4 dosage impacts cell cycle control and impinges on neurogenesis.

Homeostatic maintenance of biological systems requires that dynamic transitions be carried out efficiently and accurately. One such complex system is the mammalian cell cycle. Orchestration of its multiple components requires the concerted effort of the transcriptional, translational, and proteasomal machinery. The regulation of protein stability by post-translational modifications is especially important, as it allows for rapid control of positive and negative cell cycle regulators, both of which need to be properly controlled for smooth phase transitions.

Many key cell cycle proteins are phosphorylated on specific residues prior to proteasomal degradation. These "marked" substrates are sensed by an F-box protein component of the conserved SCF family of E3 ubiquitin ligases, ubiquitinated, and subsequently degraded by the proteasome (1–3). Of the numerous mammalian F-box proteins that exist, FBW7, SKP2, and β-TrCP have well established roles in the degradation of cell cycle proteins. In particular, cyclins, phosphatases, and cyclin-dependent kinase (CDK)[3] inhibitors are established substrates of these effectors (4, 5).

Although site-specific phosphorylation is an underlying theme in protein degradation, reports of multisite phosphorylation converging to control specific responses are emerging. In *Saccharomyces cerevisiae*, the CDK inhibitor Sic1 is targeted for degradation by charging a minimum of 6 proline-directed phosphoacceptor sites. Subsequently, Sic1 is efficiently bound by the F-box protein Cdc4, ubiquitinated, and degraded by the proteasome. This type of threshold response creates a decisive, ultrasensitive switch for the G_1/S transition (6). In contrast, graded responses allow for fine-tuning of specific activities. For example, multisite phosphorylation impacts the DNA binding affinity of the transcription factor Ets-1 (7). The "rheostat" behavior that additive phosphorylation confers allows for precise tuning of its transcriptional activity. A recent report on cell cycle control by mitogen-activated protein kinase during yeast differentiation also attests to the importance of graded responses by multisite phosphorylation (8).

Extensive cell proliferation and cell cycle control are fundamental features of mammalian development. In particular, neural progenitor proliferation during embryonic brain development requires precise balancing with neural differentiation. Perturbations in the cell cycle/proliferation machinery affect the orderly process of brain development and impacts final organ size. Along these lines, transgenic mice expressing stabilized β-catenin, a model for constitutive Wnt signaling, exhibit a profound increase in brain size (9). In addition to proliferative signaling, directly impacting the mitotic apparatus can influence neural progenitor proliferation and differentiation (10, 11). Although reports detailing responses of neural progenitors to proliferative signaling and cell fate determinants are relatively abundant, only a few studies have linked defects in the cell cycle machinery to disruptions in brain development.

In this study, we link multisite phosphorylation-dependent degradation of the mammalian protein activating transcription factor 4 (ATF4) and its effect on cell cycle progression to

* This work was supported by RIKEN and the Howard Hughes Medical Institute.

⌘ *Author's Choice*—Final version full access.

[S] The on-line version of this article (available at http://www.jbc.org) contains supplemental Figs. S1–S5.

[1] Both authors contributed equally to this work.

[2] Investigator of Howard Hughes Medical Institute. To whom correspondence should be addressed: 77 Massachusetts Ave., Cambridge, MA 02115. Tel.: 617-324-1660; Fax: 617-324-1667; E-mail: lhtsai@mit.edu.

[3] The abbreviations used are: CDK, cyclin-dependent kinase; ATF4, activating transcription factor 4; CK1, casein kinase 1; PDP, proline-directed phosphorylation; VZ, ventricular zone; IZ, intermediate zone; CP, cortical plate; CIP, calf intestine phosphatase; CREB, cAMP-response element-binding protein.

describe a novel mechanism regulating embryonic neurogenesis. ATF4, a member of the ATF family of basic leucine zipper transcription factors, exerts its influence in stress response (12, 13), development (14–17), and learning and memory (9, 18, 19). Although translation of the ATF4 message is a well established mechanism for increasing ATF4 expression (12, 20), we provide evidence of a mechanism that requires multiple phosphorylation events to converge on a β-TrCP degron to control ATF4 stability. We find that a proline-directed phosphorylation (PDP) gradient influences multiple aspects of ATF4 stability, including binding to the F-box protein β-TrCP2, ubiquitination, and phosphorylation of the β-TrCP degron. ATF4 was found to be highly expressed in neural progenitors in the embryonic neocortex, and its persistence caused cells to accumulate in early G_1 and repressed neurogenesis. Importantly, we demonstrate that neural progenitors are acutely sensitive to ATF4 dose and that proper control of ATF4 levels is required for efficient neurogenesis in the developing mouse brain.

EXPERIMENTAL PROCEDURES

Materials—The following chemicals were used for this study: thymidine (Calbiochem), nocodazole (Sigma), aphidicolin (Sigma), MG132 (Sigma), IC261 (Sigma), cycloheximide (Sigma), BrdU (Sigma), and calf intestine alkaline phosphatase (CIP) (New England Biolabs).

Cell Culture/Transfection/Synchronization—HeLa, 293T, and NIH3T3 cells were maintained in DMEM (Invitrogen) supplemented with 10% FBS and antibiotics. NIH3T3 cells were synchronized at the G_1/S phase using aphidicolin (5 μg/ml) for 20 h. S-phase-enriched cells were obtained by treating with 2.5 mM thymidine for 20 h. M-phase cells were obtained by treating with nocodazole for 20 h followed by shake off. The quality of synchronization was confirmed by flow cytometry. NIH3T3 cells were arrested in early S-phase using a double thymidine block and released with 2 washes in PBS prior to addition of fresh medium.

Constructs—ATF4 and its mutant variants were cloned into a pcDNA-3×FLAG vector containing three tandem copies of the FLAG epitope coding sequence at the N terminus and the pCAG-IRES-EGFP vector. The various serine to alanine mutants were generated using a PCR-based mutagenesis strategy and verified by sequencing. Primer sequences are available upon request.

Antibodies—Antibodies used in this study include: anti-FLAG M2 from Sigma, anti-ATF4 from Santa Cruz (Santa Cruz Biotechnology, Santa Cruz, CA), anti-ATF4 developed in rabbits immunized with the first 272 amino acids of mouse ATF4, anti-ATF4-S218P, anti-γ-tubulin from Sigma, anti-actin from Sigma, anti-proliferating cell nuclear antigen and anti-cyclin B from Santa Cruz, anti-GST from Cell Signaling, anti-myc, anti-ubiquitin, anti-p35, and anti-CDK5 from Santa Cruz, anti-cyclin D (DCS6) from Cell Signaling, anti-Ki-Mcm6 from BD Bioscience, anti-cleaved caspase 3 from Cell Signaling, and anti-Tbr1 from Abcam.

Western Blot/Immunoprecipitation—For detection of endogenous ATF4, nuclear or RIPA extracts were prepared. For nuclear extracts, 10-cm dishes of 3T3 cells were initially treated with Buffer A consisting of 0.05% Triton, 20 mM HEPES, pH 7.9, 10 mM KCl, 1 mM DTT, EDTA, EGTA, protease inhibitor mixture (Roche Applied Science), sodium fluoride, β-glycerol phosphate, and sodium pyrophosphate for 10 min on ice. Following 2 washes in the same buffer, the nuclear proteins were extracted with Buffer B consisting of 10 mM HEPES, pH 7.9, 500 mM NaCl, 1 mM DTT, EDTA, EGTA, protease inhibitor mixture, NaF, β-glycerol phosphate, and sodium pyrophosphate. Nuclear proteins (20 μg) were loaded for Western blot. To determine Ser^{218} phosphorylation of endogenous ATF4 in brains, E12 mouse brains were pooled and lysed in RIPA buffer. Lysates (500 μg) were subjected to ATF4 or HA immunoprecipitations in RIPA buffer with ATF4 or HA antibody cross-linked Protein A beads followed by Western blot analysis with S218P and ATF4 antibodies. Immunoprecipitations for protein-protein interactions were performed in immunoprecipitation buffer consisting of 0.6% Triton, 150 mM NaCl, 50 mM Tris, pH 7.5, protease inhibitors, and phosphatase inhibitors. FLAG immunoprecipitations and glutathione *S*-transferase (GST) pulldowns were performed using M2 FLAG-agarose-conjugated resins (Sigma) and glutathione-Sepharose beads (Roche), respectively. To detect Ser^{218} phosphorylation and ubiquitination of exogenous ATF4, FLAG-tagged ATF4 mutants were immunoprecipitated and washed in RIPA buffer followed by Western blot analysis.

Alkaline Phosphatase Treatment—Cells were lysed in buffer containing 0.5% Triton, 50 mM Tris, pH 8.0, 150 mM NaCl, and protease inhibitors. Equal amounts of lysates were diluted in the same buffer without Triton X-100 and treated with 5 units of CIP (New England Biolabs) for 1 h at 37 °C. SDS sample loading buffer was added to terminate the reaction and lysates were analyzed by Western blot.

ATF4 Stability Assays—The stability of the various forms of ATF4 was determined by treating cells transfected with the various FLAG-tagged ATF4 mutants with cycloheximide for the indicated durations. The amount of plasmid transfected was optimized so that the endogenous ubiquitination and proteasome machinery efficiently degraded WT ATF4 in 293T cells during the time frame observed. Lysates were subjected to Western blot analysis and the resulting band intensities were determined by densitometry. A WT ATF4 series was included in all experiments for quality control. Results are plotted as the mean of at least three independent experiments.

Retroviral Transduction—The various ATF4 mutants were cloned into the pMSCV-puro (Clontech) vector. Retrovirus was packaged in Phoenix cells and viral supernatant was collected at 8-h intervals over the course of 4 days. For transduction of NIH3T3 and N2A cells, culture medium was replaced with viral supernatant in the presence of Polybrene for 16 h. Following 24 h of recovery, infected cells were selected with puromycin (1 μg/ml) over the course of 4 days. Cell cycle analysis was performed by plating a fixed number of selected cells into 24-well plates on coverslips and processing by immunohistochemistry as described below. Cell counts were performed by plating 4×10^4 cells/well in triplicate in 6-well plates over the course of 7 days. Cells were trypsinized and counted with a hemocytometer.

In Utero Electroporation/Immunohistochemistry—*In utero* electroporations of E11.5–E12 embryos were performed on

pregnant Swiss Webster mice as described previously (21). Animal experiments were approved by the Massachusetts Institute of Technology Committee on Animal Care. Cryosections (12 μm) generated from fixed brains were subjected to fluorescent immunohistochemistry. Antibodies used were: anti-GFP polyclonal antibody (Molecular Probes, Aves labs), anti-Tuj1 monoclonal antibody (Covance), anti-Ki-Mcm6 (BD Biosciences), anti-Ki-67 (Neomarkers), and anti-Nestin monoclonal antibody (Pharmingen). Secondary antibodies used were goat anti-rabbit Cy2 and Cy3 and goat anti-mouse Cy2, Cy3, and Cy5 (Jackson ImmunoResearch). Images were acquired on a laser scanning confocal microscope (LSM 510; Carl Zeiss MicroImaging, Inc.) and processed using LSM image browser version 4.2 (Carl Zeiss MicroImaging, Inc.).

ATF4 and Phosphor-Ser^{218} Antibody—To generate the polyclonal ATF4 antibody, rabbits were immunized with a fragment of murine ATF4 spanning amino acids 1–272 fused to GST. Specific antibodies were purified by first clearing with a GST column, followed by purification with GST-ATF4. To generate the phosphoserine 218 antibody, rabbits were immunized with the peptide PSDNDSGICMSP (underlined serine is phosphorylated). Phosphorylation specific antibody was purified from crude rabbit serum using the Sulfolink kit (Pierce) conjugated with the phosphopeptide used for immunization after preclearing serum with a non-phosphorylated peptide.

Kinase Assay—Cold kinase assays were performed in the presence of Cdc2 kinase buffer (New England Biolabs), 100 mM ATP, 50 units of casein kinase (CK) 1 (New Engalnd Biolabs) and CK2 (New Engalnd Biolabs) (with or without Cdc2/cyclin B), and 100 ng of purified GST-ATF4. Reactions were performed at room temperature for 1 h and terminated by addition of SDS sample buffer and boiling. Samples were analyzed by Western blot analysis with anti-S218P.

Cell Cycle/Fluorescence-activated Cell Sorting (FACS) Analysis—Asynchronously growing NIH3T3 cells were transfected with the various pCAG-IRES-EGFP based constructs for 48 h prior to determining the BrdU labeling and mitotic index. For BrdU labeling experiments, a 1-h pulse of 20 μM BrdU was applied to the cells prior to fixation. Once fixed, cells were treated with 2 N HCl for 20 min, and processed for immunocytochemistry with antibodies against GFP (Molecular Probes) and BrdU (DAKO). For mitotic index studies, transfected cells were processed and stained with an antibody against phosphohistone H3 (Upstate). Early G_1 arrest was determined using antibodies against Ki-67 (Neomarkers) and Ki-Mcm6 (BD Biosciences). For FACS analysis, cells were transfected with the indicated plasmids for 48 h. Cells were fixed with 2% paraformaldehyde for 7 min, washed several times, and permeablized with 75% ethanol overnight. Cells were washed free of ethanol, incubated with RNase and propidium iodide for 30 min at 37 °C, and analyzed with a FACScan machine. Cells were gated for GFP expression, and the DNA content of at least 15,000 GFP positive cells were analyzed for each sample using ModFit.

In Situ Hybridization—Embryos aged E12.5 and E16.5 were isolated from ATF4 ± heterozygous crosses and genotyped. Embryonic brains were fixed in 4% paraformaldehyde overnight followed by cryoprotection with 30% sucrose/PBS overnight, and sectioning (12 μm) with a cryostat. Knock-out brains and embryos were used as negative controls. Digoxigenin RNA probes to mouse ATF4 (879 bp fragment) were generated using a probe synthesis kit (Roche Applied Science), hybridized overnight, and brains were incubated with an alkaline phosphatase-conjugated antibody against digoxigenin (Roche Applied Science) following probe hybridization. Sections were developed using a combination of nitro blue tetrazolium and 5-bromo-4-chloro-3-indolyl phosphate reagents (Roche Applied Science) for 6 h at room temperature.

RT-PCR Analysis—Total mRNA was isolated from embryonic mouse brains at various developmental stages (E11 to adult) using the RNeasy minikit (Qiagen). cDNA was prepared with oligo$(dT)_{20}$ primers using the SuperScript III first strand synthesis kit (Invitrogen). Semi-quantitative PCR was performed using the Quick Load *Taq* 2× master mix (Invitrogen). 25 cycles of amplification were performed for ATF4 and actin. Actin primers were: 5′-CGTGGGCCGCCCTAGGCACCA-3′ and 5′-TTGGCCTTAGGGTTCAGGGGGG-3′. ATF4 primers were 5′-TAGATGACTATCTGGAGGT-3′ and 5′-TGGTTTCCAGGTCATCCATT-3′. PCR products were resolved on 1% agarose gels and visualized by ethidium bromide staining.

Luciferase Assay—Luciferase assay was performed with the dual luciferase assay kit (Promega). NIH3T3 cells were cotransfected with ATF4, cyclin D1 promoter (41), and SV-40 promoter-driven *Renilla* luciferase control for 24 h. Assays were carried out with a LMAXII luminometer (Molecular Devices).

RESULTS

ATF4 Is Phosphorylated and Its Levels Oscillate during the Cell Cycle—We initially developed an interest in a role for ATF4 during the cell cycle based on its spatiotemporal expression during neurodevelopment. ATF4 is abundantly expressed in neural progenitors of the cortical ventricular zone (VZ) during a period of extensive progenitor pool expansion (Fig. 6, *A* and *B*), potentially implicating it in proliferation and cell cycle control. Because ATF4 is ubiquitously expressed in tissues and its potential role in proliferation is likely conserved in cycling cells, we turned to a heterologous system to gain mechanistic insight into its regulation during the cell cycle. In chemically synchronized cells, endogenous ATF4 levels were highest in S-phase (Fig. 1*A*) and less detectable in M-phase and G_1. Furthermore, we discovered that ATF4 is phosphorylated during the cell cycle, as demonstrated by the increased mobility after alkaline phosphatase (CIP) treatment (Fig. 1*B*). The decline in ATF4 levels as cells approach G_2/M was clearly observed after release from a double thymidine block (Fig. 1*C*). These results suggest that ATF4 is phosphorylated, highly expressed during S-phase, and oscillates during the cell cycle.

Our observation that ATF4 is phosphorylated during the cell cycle prompted investigation into the specific sites that were phosphorylated. Overexpression of ATF4 revealed a mobility shift that was ablated upon alkaline phosphatase treatment, suggesting that exogenous ATF4 is efficiently phosphorylated by endogenous kinases (Fig. 1*D*). To characterize the phosphorylation events, ATF4 truncations were generated and tested for the mobility shift. Of the truncations tested, only the fragment spanning amino acids 190–272 exhibited a mobility shift sensitive to CIP treatment. Interestingly, this fragment contains

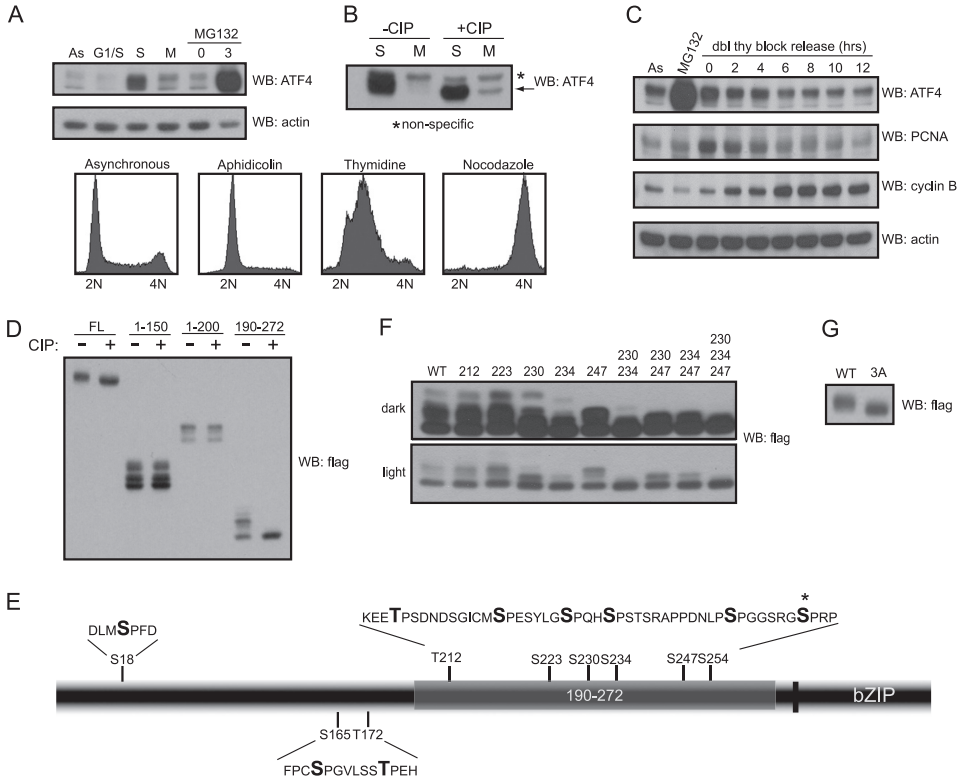

FIGURE 1. **ATF4 levels oscillate during the cell cycle.** *A*, lysates from synchronized NIH3T3 cells were immunoblotted with the indicated antibodies. Degree of synchrony was confirmed by flow cytometry. As a control, MG-132 was used to stabilize endogenous ATF4. *As*, asynchronous; G_1/S, G_1 phase/S-phase; *S*, S-phase; *M*, mitosis. *B*, lysates from NIH3T3 cells synchronized in S-phase (*thymidine*) and M-phase (*nocodazole*) were subjected to alkaline phosphatase treatment (+*CIP*). *C*, NIH3T3 cells synchronized in early S phase with a double thymidine block were released for the indicated durations. Nuclear extracts were collected and immunoblotted with the indicated antibodies. *D*, HEK293T cells were transfected with the indicated ATF4 truncation constructs. Lysates were collected, subjected to CIP treatment, and immunoblotted with FLAG antibody. *E*, schematic of potential proline-directed serines and threonines in murine ATF4. *Asterisk*, the proline following Ser^{254} is not conserved across species. *F*, HEK293T cells were transfected with mutant variants of the 190–272 fragment and full-length ATF4 as indicated and subjected to immunoblot analysis with FLAG antibody. *Light*, light exposure; *dark*, dark exposure. *G*, lysates from 293T cells transfected with full-length WT or triple mutant (*3A*) ATF4 were subjected to immunoblot analysis with FLAG antibody. *WB*, Western blot.

multiple PDP sites that potentially serve as substrates for cell cycle kinases (Fig. 1*E*). Mutations of the proline-directed sites to alanine revealed that mutation of a combination of three sites (Ser^{230}, Ser^{234}, and Ser^{247}) was required to completely abolish the shift (Fig. 1*F*). Importantly, this could be recapitulated in the full-length protein (Fig. 1*G*), suggesting that ATF4 is phosphorylated by endogenous proline-directed kinases on at least three residues.

ATF4 Stability Is Regulated by a Gradient of Phosphorylation—The F-box protein β-TrCP binds to and targets ATF4 for ubiquitin-dependent proteolysis (22, 23). The interaction requires phosphorylation of the first serine in the degron motif ($DSGX_nS$) corresponding to Ser^{218} in mouse ATF4. Interestingly, the degron resides within the 190–272 fragment and hinted that the three mapped PDP sites might affect ATF4 stability by regulating the phosphorylation or β-TrCP recognition of the degron. Mutation of the 3 mapped sites (230/234/247) significantly increased stability compared with wild type (WT) ATF4, but did not resemble the marked stability conferred by the degron (S218A) mutant (Fig. 2, *A* and *B*). This intermediate effect led us to investigate whether other proline-directed sites might contribute to ATF4 stability. To this end, the remaining sites within the 190–272 fragment (Thr^{212} and Ser^{223}) were mutated (hereby called 5A). When tested for stability, the 5A mutant displayed markedly increased stability compared with both the WT and 3A mutant. To gain further resolution of the contributions of various sites to ATF4 stability, we tested quadruple combinations (4A) of mutations. Surprisingly, we found that the effect of the mutations was not site-specific, but rather depended on the number of sites that were mutated. Single mutations had minor, variable effects on stability compared WT ATF4, whereas the triple mutant, followed by the quadruple and quintuple mutants, were increasingly stabilized regardless of the specific mutated sites. Consistent with these findings, WT, 3A, and 5A ATF4 displayed a graded increase in steady state expression (supplemental Fig. S1*A*).

The PDP sites that conferred resistance to degradation surround the β-TrCP degron. This arrangement suggested that PDP may regulate the interaction between β-TrCP and ATF4. To explore this possibility, various ATF4 mutants were tested for the capacity to interact with β-TrCP. As expected, WT ATF4 displayed a robust interaction with β-TrCP2 that was highly dependent on degron phosphorylation (Fig. 2, *C* and *D*). Consistent with the findings that the 3A ATF4 mutant is more stable than WT ATF4, the 3A mutant displayed a decreased interaction with β-TrCP2. Furthermore, the highly stable 5A mutant interacted with β-TrCP to a similar degree as the degron mutant. Other combinations of mutations did not significantly alter binding between ATF4 and β-TrCP2, suggesting that the 5 phosphorylation sites (Thr^{212}, Ser^{223}, Ser^{230}, Ser^{234}, and Ser^{247}) residing within the 190–272 fragment are required to confer optimal interaction.

We next determined whether the extent of ATF4 ubiquitination reflected the close correlation between the stability of the mutants and their capacity to interact with β-TrCP2. WT ATF4 was efficiently ubiquitinated, whereas the degron and 5A mutants displayed markedly reduced ubiquitination (Fig. 2*E*). Ubiquitination of the mutants displayed a graded decrease with increasing mutations, consistent with the graded effect on their stability. In effect, the 3A mutant was ubiquitinated less than WT ATF4, and the 5A mutant was ubiquitinated to a similar degree as the degron mutant. Taken together, these data suggest that the additive effect of PDP on ATF4 stability acts in graded fashion and directly

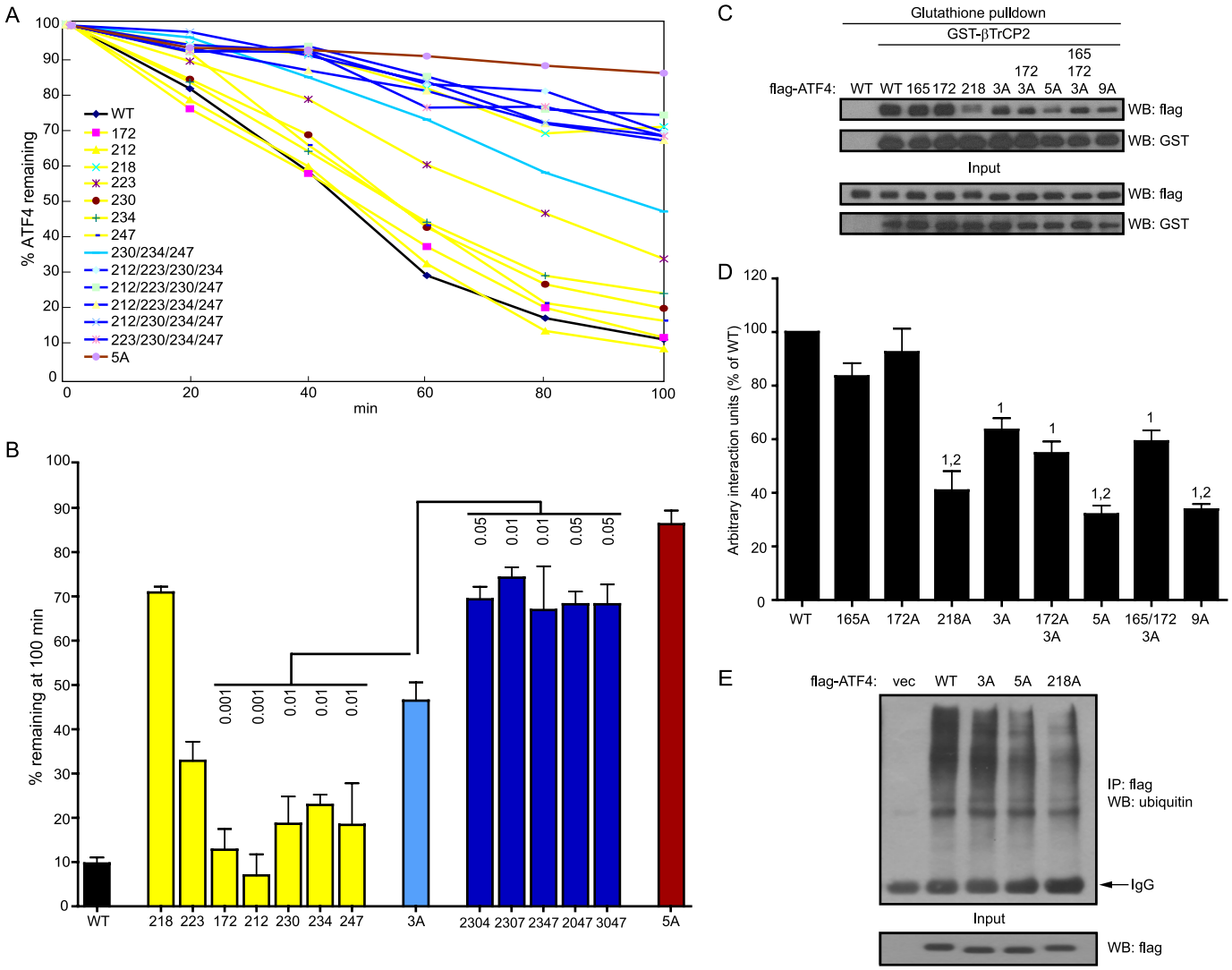

FIGURE 2. **A gradient of phosphorylation targets ATF4 for degradation by the ubiquitin proteasome system.** *A*, HEK293T cells were transfected with the indicated ATF4 constructs and treated with cycloheximide for the indicated durations. ATF4 persistence is plotted as the percentage of signal remaining compared with the vehicle-treated zero time point by densitometry. Results are plotted as the mean of at least three independent experiments. *B*, plot of percent ATF4 remaining at 100 min from *A*. Data are presented as the mean ± S.E. ($n = 3$). *p* values are denoted on the plot (one-way analysis of variance). The 4A mutants are denoted in the abbreviated form using the last number of each amino acid residue. For example, the 2304 mutant is an abbreviation for T212A/S223A/S230A/S234A. *C*, HEK293T cells were cotransfected with the indicated ATF4 mutant constructs and GST-tagged β-TrCP2 and subjected to GST pulldowns. Cells were treated with MG-132 (30 μM) prior to lysis to stabilize ATF4. The amount of ATF4 associated with β-TrCP2 was determined by Western blot analysis with FLAG antibody. *D*, quantification of *C* by densitometry presented as the mean ± S.E. *1*, $p < 0.001$ WT, 165A, 172A compared with 218A, 3A, 172/3A, 165/172/3A, 5A, and 9A; *2*, $p < 0.05$ 3A, 165/3A, 165/172/3A compared with 218A, 5A, and 9A. *p* values were obtained by one-way analysis of variance. *E*, HEK293T cells were transfected with the indicated mutant ATF4 constructs. Eighteen hours post-transfection, cells were treated with MG-132 (30 μM) for 4 h prior to lysis with RIPA buffer. Lysates were subjected to FLAG immunoprecipitation and analyzed for the degree of ATF4 ubiquitination by immunoblotting with anti-ubiquitin antibody. *WB*, Western blot.

correlates with the extent of ATF4 ubiquitination and β-TrCP interaction.

PDP Regulates the β-TrCP Degron—Our observation that the loss of PDP impacts ATF4 stability to a similar degree as the degron mutant raised the possibility of crosstalk between the two mechanisms. The β-TrCP degron in ATF4 is highly conserved (Fig. 3*A*) and Ser^{218} phosphorylation is important for generating an interaction interface for β-TrCP (Fig. 2, *C* and *D*). To test whether PDP directly influences degron phosphorylation, we generated an antibody that recognizes the first phosphorylated serine of the degron. WT ATF4 displayed robust immunoreactivity to the phospho-Ser^{218} antibody that was ablated upon CIP treatment (Fig. 3*B*). Importantly, the S218A mutant displayed no immunoreactivity. Ser^{218} phosphorylation could also be detected *in vivo* from embryonic brain lysate (supplemental Fig. S4*A*). Thus, the antibody specifically and robustly recognizes Ser^{218} phosphorylation.

We next assessed whether PDP directly regulated the degron by examining the extent of Ser^{218} phosphorylation exhibited by the various ATF4 mutants. Compared with WT ATF4, Ser^{218} phosphorylation was significantly reduced with the 3A, and decreased even further with the 5A mutant (Fig. 3, *C* and *D*). Of particular interest was the graded decrease in the contributions of the single site mutants as the distance from Ser^{218} increased ($Ser^{223} > Ser^{230} > Ser^{234} > Ser^{247}$). Although Thr^{212} impacted ATF4 stability (Fig. 2*A*), it did not affect Ser^{218} phosphorylation

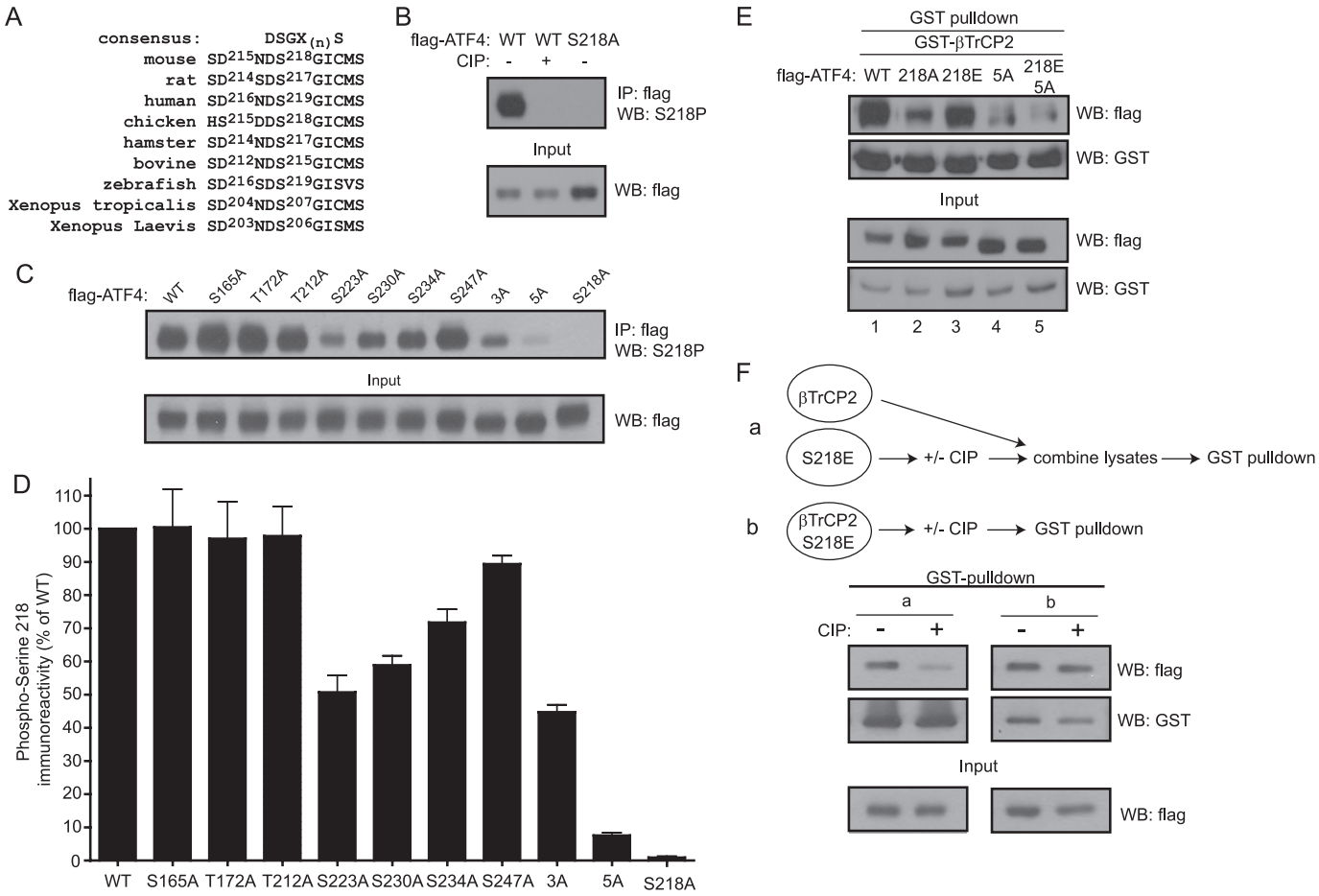

FIGURE 3. **PDP events converge to regulate phosphorylation of the β-TrCP phosphodegron.** *A*, schematic of the conserved β-TrCP degron in ATF4 across multiple species. *B*, 293T cells were transfected with the indicated FLAG-tagged ATF4 constructs. Lysates were subjected to FLAG immunoprecipitation followed by treatment with alkaline phosphatase (CIP) where indicated. Samples were then analyzed by Western blot (*WB*) using the phospho-Ser^{218} antibody. *C*, the indicated FLAG-tagged ATF4 mutants were expressed in 293T cells, which were treated with MG-132 (30 μM) for 4 h prior to lysis with RIPA buffer. Subsequently, lysates were subjected to FLAG immunoprecipitation and Western blot with phospho-Ser^{218} antibody. *D*, quantification of *C* by densitometry. Data are presented as the mean ± S.E. ($n = 3$). *E*, 293T cells were transfected with the various ATF4 mutant constructs and GST-tagged β-TrCP2 and treated with MG-132 (30 μM) for 4 h prior to lysis with RIPA buffer. Lysates were subjected to GST pulldown followed by Western blot with FLAG antibody. *F*, 293T cells were transfected individually or in combination with the indicated plasmids (FLAG-S218E and/or GST-β-TrCP2) as depicted. Following CIP treatment, cell lysates were subjected to GST pulldown followed by Western blot with the indicated antibodies.

suggesting that Thr^{212} may contribute to other aspects of ATF4 degradation.

The spatial correlation between the distance from the degron and the degree of Ser^{218} phosphorylation/β-TrCP binding suggested that the β-TrCP interaction may be influenced by local conformational changes. To test this hypothesis, we determined whether the compounded alanine mutations still affected β-TrCP binding when the degron is constitutively charged. We first confirmed that a glutamic acid substitution of the serine in the degron (S218E) supports the β-TrCP interaction (Fig. 3*E*). We next compounded the S218E mutation onto the 5A mutant to generate a 5A-S218E mutant. Importantly, this mutant (*lane 5*), regardless of the constitutively charged state of the degron, displayed an inefficient interaction with β-TrCP similar to that observed with the 5A mutant (*lane 4*). This result supports the notion that local conformational changes around the degron are required for the β-TrCP interaction.

Further evidence for a conformational change was obtained using a modified GST pulldown scheme (Fig. 3*F*). Cells were either transfected individually or co-transfected with β-TrCP and the constitutively charged degron mutant (S218E). In the individually transfected set, S218E expressing cell lysates were treated with or without CIP prior to combining with the β-TrCP containing lysate. Binding of CIP-treated S218E to β-TrCP was inefficient, consistent with the notion that either the phosphorylation events directly play a role in the interaction, or that a conformational change required by PDP did not occur to allow for degron recognition. To distinguish between these two possibilities, we co-transfected cells with the S218E mutant and β-TrCP and treated lysates with or without CIP prior to GST pulldown. Consistent with a conformational change, abolishing PDP with CIP treatment after the interaction between β-TrCP and S218E took place (in cells) did not adversely affect the interaction. This supports the model that PDP is initially required to provide access to the degron, and that it is dispensable once the interaction has taken place.

A key unresolved issue regarding β-TrCP-mediated ATF4 degradation is the identity of the Ser^{218} kinase. To approach this, we screened a panel of kinases for the ability to phosphor-

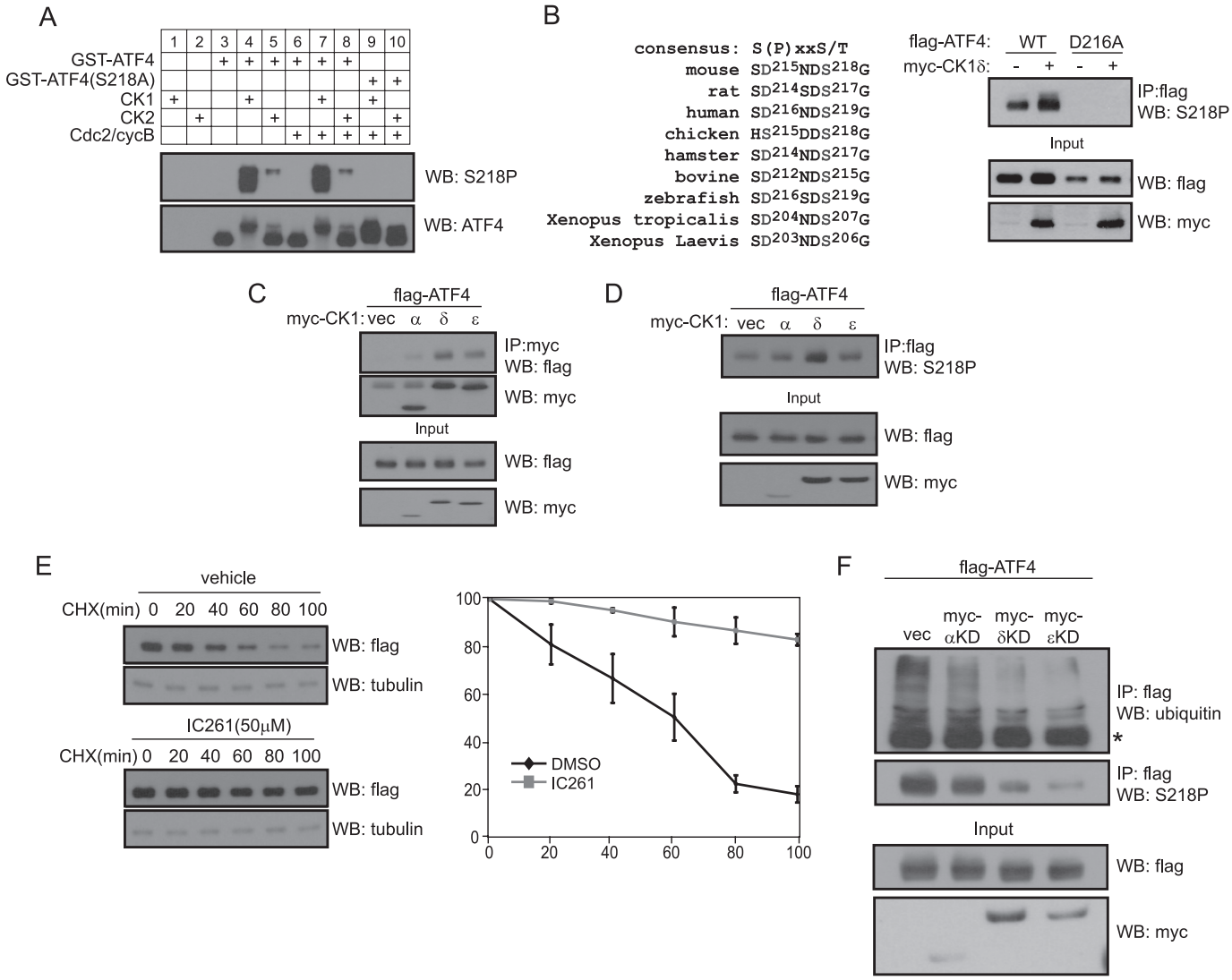

FIGURE 4. **CK1 regulates ATF4 stability.** *A*, cold *in vitro* kinase assay with purified GST-ATF4 and CK1, and CK2 kinases. Samples were analyzed by immunoblotting with the Ser^{218} phospho-specific antibody. *B*, FLAG-tagged ATF4 or the corresponding D216A mutant were transfected into 293T cells. Following FLAG immunoprecipitation with cell lysates, immunoprecipitates were subjected to Western blot with the phospho-Ser^{218} antibody. *C*, FLAG-tagged ATF4 and myc-tagged CK1 α, δ, or ϵ were transfected into 293T cells and cells were treated with MG-132 for 4 h prior to lysis. Following FLAG immunoprecipitation, immunoprecipitates were subjected to Western blot (*WB*) with the indicated antibodies. IgG heavy chain overlaps with myc-tagged CK1δ and -ϵ. *D*, FLAG-tagged ATF4 and myc-tagged CK1 were transfected into 293T cells as in *C*. Phosphorylation of the Ser^{218} residue was analyzed by FLAG immunoprecipitation followed by Western blot with the S218P antibody. *E*, stability of ATF4 in cells pretreated with 50 μM IC261 was analyzed as described in the legend to Fig. 2*A*. The exposure was adjusted to achieve comparable starting ATF4 levels for both samples. *F*, 293T cells were co-transfected with FLAG-tagged ATF4 and dominant-negative CK1 constructs and treated with MG-132 for 4 h prior to lysis. Lysates were subjected to FLAG immunoprecipitation followed by Western blot (*WB*) with ubiquitin and S218P antibodies. The *asterisk* represents monoubiquitinated ATF4. *CHX*, cycloheximide.

ylate the degron (Fig. 4*A*). *In vitro* kinase assays revealed casein kinase 1 (CK1) (*lane 4*), and to a lesser extent casein kinase 2 (CK2) (*lane 5*), as Ser^{218} kinases. Other kinases, including Cdc2/cyclin B, Plk1, GSK3β, and Chk1, did not phosphorylate Ser^{218} under the conditions tested (data not shown). Importantly, Ser^{218} phosphorylation was not observed in the S218A mutant (*lane 9*). Phosphorylation by CK2 was inefficient and likely represented nonspecific phosphorylation (*lane 5*). Although Ser^{218} does not conform to a CK2 consensus site, (S/T)*XX*(D/E), it does somewhat resemble the CK1 consensus, p(S/T)*XXX*(S/T), where the first phosphorylated residue primes CK1 activity. The position of the priming residue in ATF4 coincides with a conserved aspartic acid residue, an acidic residue that can mimic phosphorylation (Fig. 4*B*). Consistent with this, mutation of the conserved Asp^{216} residue to alanine completely abolished degron phosphorylation (Fig. 4*B*).

Based on our *in vitro* kinase assay, we directed our attention to functional and biochemical interactions between ATF4 and CK1 in cells. When co-expressed in 293T cells, ATF4 preferentially interacted with the δ/ϵ family of CK1 kinases (Fig. 4*C*). Importantly, this interaction was independent of PDP (supplemental Fig. S1*B*), implying that CK1 recruitment is independent of these modifications. We also recapitulated Ser^{218} phosphorylation by CK1 in cells; CK1δ markedly elevated Ser^{218} phosphorylation, although both CK1α and CK1ϵ mildly increased Ser^{218} phosphorylation (Fig. 4*D*). To expand on these results, we determined whether inhibiting CK1 activity affected ATF4 stability. Pretreatment of cells with a specific

pharmacological inhibitor of CK1δ/ϵ, IC261, markedly stabilized exogenous ATF4 (Fig. 4*E*). Importantly, coexpression of dominant-negative CK1δ and -ϵ (both inhibit CK1δ/ϵ isoforms) with ATF4 resulted in significantly decreased ubiquitination and Ser^{218} phosphorylation (Fig. 4*F*).

ATF4 Degradation Is Required for Efficient Cell Cycle Progression—Based on the oscillating expression of ATF4 during the cell cycle, we hypothesized that this oscillation, controlled in part by degradation, is important for cell cycle progression. Thus, overriding the oscillations by introducing stabilized mutants may impact the cell cycle. We initially determined whether the degradation mutants affected DNA replication and mitotic entry. To this end, we transfected NIH3T3 cells with ATF4 mutant constructs and determined the BrdU labeling and the mitotic indexes (phospho-histone H3 labeling). WT ATF4 significantly decreased both the BrdU labeling (Fig. 5*A*) and mitotic index (Fig. 5*B*) compared with the control. Importantly, the stabilized mutants S218A and 5A had a greater impact than WT ATF4 on both indexes. The observed decrease in proliferation suggested that stabilized ATF4 expressing cells undergo cell cycle arrest. To examine this, we performed flow cytometry analysis on asynchronously growing HeLa cells transfected with the stabilized mutants. We chose HeLa cells based on the equal distribution of cells in the various phases of the cell cycle compared with the relatively G_0/G_1 enriched content of NIH3T3 cells (data not shown). Cell cycle distributions of GFP-positive cells revealed that whereas WT ATF4 had no discernable effect on the distribution, S218A and 5A mutants substantially increased the portion of cells in G_0/G_1 compared with the control (Fig. 5*C*).

To gain further resolution on the G_0/G_1 block, we stained cells with Ki-Mcm6, a marker expressed during all phases of the cell cycle (except G_0) (24), and Ki-67, which is expressed in all phases of the cell cycle except early G_1. In asynchronous cultures, virtually all cells are Ki-Mcm6 positive, whereas ~85% of cells are Ki-67 positive, suggesting that ~15% of cells are in early G_1. We initially ruled out the possibility that cells exited the cell cycle and entered a quiescent state based on the positive staining of stabilized ATF4-transfected cells for Ki-Mcm6. We also ruled out a loss of Ki-67 immunoreactivity as a general phenomenon of cell cycle arrest because cells that were chemically arrested (at G_1/S, S, or M-phase) remained Ki-67 positive (supplemental Fig. S2). Taking advantage of the Ki-Mcm6/Ki-67 double staining scheme, we determined the percentage of cells accumulating in early G_1. Cells in early G_1 would stain positively for Ki-Mcm6 but be Ki-67 negative. Although WT ATF4 expressing cells moderately increased cells accumulating in early G_1 compared with the control, the S218A and 5A mutants potently induced early G_1 accumulation (Fig. 5*D*).

To control for the possibility that ATF4-expressing cells arrest due to non-physiological overexpression of exogenous ATF4, we performed the same experiments using retroviral expression. Importantly, exogenous ATF4 was expressed at comparable levels to endogenous ATF4 (supplemental Fig. S3*A*). We observed similar profiles for BrdU, mitotic, and early G_1 arrest indexes (supplemental Fig. S3, *B–D*), suggesting that the cell cycle phenotypes observed with overexpression mimic that of exogenous ATF4 expressed at endogenous levels. Furthermore, we observed a graded decrease in proliferation as assessed by cell counts in retroviral-mediated WT and stabilized-ATF4 expressing NIH3T3 cells (Fig. 5*E*). These data demonstrate that the cell cycle is sensitive to ATF4 dosage and that ATF4 persistence elicits early G_1 arrest.

ATF4 Is Expressed in the VZ during Embryonic Brain Development—Numerous studies have documented functions for ATF4 in the mature central nervous system (9, 18, 19, 25–29); however, no role or characterization of ATF4 function in the developing embryonic brain has been described. *In situ* hybridization of brain sections from embryos of various developmental stages revealed that ATF4 is expressed early during cortical brain development (Fig. 6*A*). Importantly, ATF4 expression was not observed in neurons at this stage. To gain better spatial resolution, we analyzed brains from a later stage when neurons are abundant. *In situ* hybridization of E16.5 brains revealed that ATF4 was most highly expressed in the proliferative VZ, consistent with its expression pattern at E12.5. However, ATF4 was also observed in the CP, suggesting that its expression is reactivated in mature neurons. To determine whether ATF4 protein expression mirrored that of its message, lysates from brains of various developmental stages were analyzed (Fig. 6*B*). ATF4 protein is most highly expressed early in brain development during a period mainly characterized by progenitor proliferation. ATF4 levels decline as neurogenesis increases (at around E11) as demonstrated by increased expression of p35, the neuron-specific activator of the CDK5 kinase. The decrease in ATF4 levels likely reflects the gradual depletion of the progenitor pool and increase in neurons as neurogenesis proceeds. It also suggests that ATF4 might be subject to post-transcriptional or post-translational control in neurons, as the protein levels did not exhibit a commensurate increase consistent with the expression of ATF4 message in the CP.

ATF4 Degradation Is Required for Proper Cell Positioning during Neurodevelopment in Vivo—To determine whether ATF4 degradation is required for cell cycle progression *in vivo*, we utilized the *in utero* electroporation technique (Fig. 6*C*). We electroporated E11.5–E12 embryos based on the temporal expression pattern of ATF4 and technical difficulty of performing electroporations on earlier embryos. We initially determined the positioning of cells (VZ, IZ, or CP) expressing the various ATF4 mutants relative to WT ATF4 and the GFP control 2 days post electroporation (E13.5–E14). Although WT ATF4 caused a significant increase in cells accumulating in the VZ compared with the GFP control, the stabilized mutants had a more potent effect (Fig. 6, *D* and *E*). Correspondingly fewer cells entered the IZ and CP in both WT and stabilized ATF4-electroporated brains. These results imply a defect in the cell cycle or differentiation of the neural progenitors. Alternatively, progenitors may differentiate into neurons, but have migration defects that preclude efficient exit from the VZ.

Early G_1 Block Results in Decreased Neurogenesis in Vivo—We initially addressed whether cells accumulated in the VZ due to a neuronal migration defect by determining whether the cells had differentiated into neurons. To this end, we determined the fraction of GFP-positive cells that were positive for the early neuron marker Tuj1 (Fig. 7*A*). Although a few Tuj1 positive neurons could be observed in the VZ, none were GFP positive.

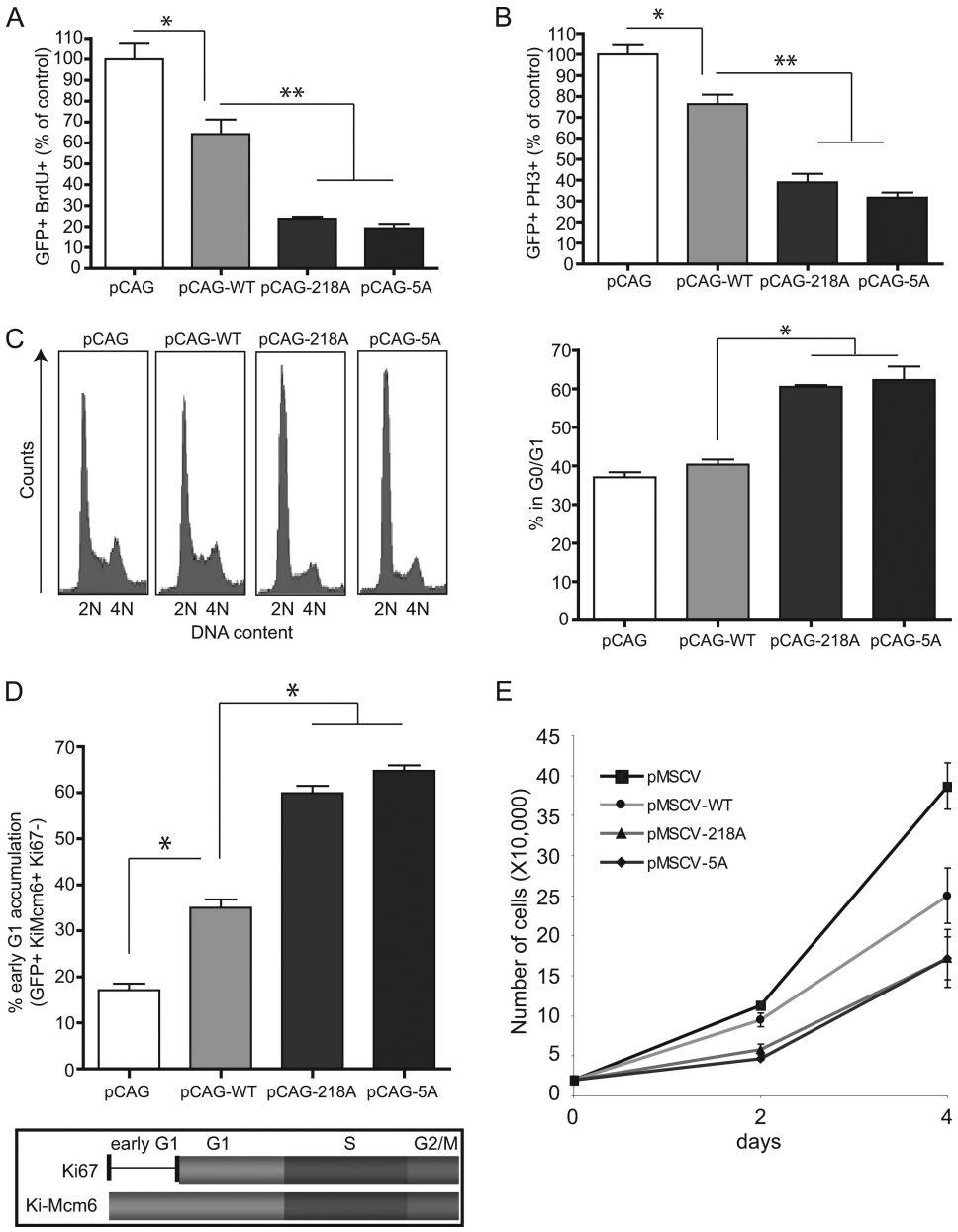

FIGURE 5. **Stabilized ATF4 induces an early G_1 cell cycle arrest.** *A*, NIH3T3 cells were transfected with the indicated pCAG-IRES-GFP plasmids for 48 h. Cells were given a 20 μM BrdU pulse for the last hour, fixed with antibodies against GFP and BrdU. Presented is the percentage of GFP and BrdU double positive cells. BrdU incorporation for the control (*pCAG*) was set to 100% and other samples were normalized to the control. Data are presented as the mean ± S.E. ($n = 3$). *, $p < 0.01$; **, $p < 0.001$ (one-way analysis of variance). *B*, NIH3T3 cells were transfected as in *A*. Mitotic cells were analyzed by costaining with antibodies against GFP and phosphohistone H3 antibodies. Data are presented as the mean ± S.E. ($n = 3$). *, $p < 0.01$; **, $p < 0.001$ (one-way analysis of variance). *C*, FACS analysis of HeLa cells transfected with the indicated plasmids. GFP-positive cells were gated and analyzed for DNA content. *Below*, quantification of the percent of G_0/G_1 cells from *C*. Data are presented as the mean ± S.E. ($n = 3$). *, $p < 0.001$ (one-way analysis of variance). *D*, NIH3T3 cells were transfected with the indicated plasmids and stained with Ki-Mcm6 and Ki-67 antibodies. Early G_1 arrest is calculated as the ratio of GFP + Ki-Mcm6 + Ki67, to total GFP + Ki-Mcm6 + cells. Data are presented as the mean ± S.E. ($n = 3$). *, $p < 0.001$ (one-way analysis of variance). *E*, NIH3T3 cells infected with retrovirus encoding the indicated variants of ATF4 were selected by puromycin for 3 days. Cells were replated at 20,000 cells per well, and cell number was counted over the course of 4 days.

This suggested that the GFP-positive cells blocked in the VZ did not become neurons. In addition, GFP-positive cells analyzed for the control, WT ATF4, S218A mutant, and 5A mutant exhibited a distribution of neurons consistent with the positioning experiment. Furthermore, staining with a progenitor marker (nestin) revealed that GFP-positive cells accumulating in the VZ were progenitors (supplemental Fig. S4*B*). These data suggest that cells expressing stabilized ATF4 accumulating in the VZ retain progenitor identity and that the defect is one inherent to progenitors.

Based on our results from cell lines, we hypothesized that the positioning defect may be due to an early G_1 block in the progenitor cell cycle. We coupled immunohistochemical detection of Ki-67 and Ki-Mcm6 to determine the fraction of GFP-positive cells arrested in early G_1 as mentioned previously. The specificity of the Ki-Mcm6 antibody for labeling progenitors was confirmed in cultured cortical cells (supplemental Fig. S4, *C* and *D*). In brain sections, we confirmed a significant overlap between expression of Ki-Mcm6 and Ki-67 in the VZ (supplemental Fig. S4*E*). Electroporation of stabilized mutants S218A and 5A resulted in a robust increase in the percentage of GFP-positive cells in the VZ that accumulated in early G_1 compared with control GFP-electroporated brains (Fig. 7*B*). WT ATF4 electroporated brains exhibited an intermediate effect. These data suggest that the requirement for control of ATF4 levels is conserved *in vivo* and may impact the neurogenic program.

ATF4-induced Cell Positioning and Neurogenesis Defects Derive from an Underlying Cell Cycle Defect—Our hypothesis was that stabilized ATF4 expressing cells remain progenitors and accumulate in early G_1, resulting in decreased neurogenesis. However, another possibility is that ATF4 represses neurogenic genes. During the course of our studies, we found that stabilized ATF4 suppressed cyclin D expression in NIH3T3 cells, ATF4 reduced cyclin D promoter activity, and cyclin D coexpression overrode ATF4-mediated early G_1 arrest and restored cell proliferation (supplemental Fig. S5, *A–D*). This finding provided us with a unique opportunity to address this issue. If the neurogenesis defect is cell cycle based, cyclin D expression should restore proliferation and thus neurogenesis. If the defect is an impaired differentiation program, cyclin D expression should not rescue neurogenesis. Upon cyclin D

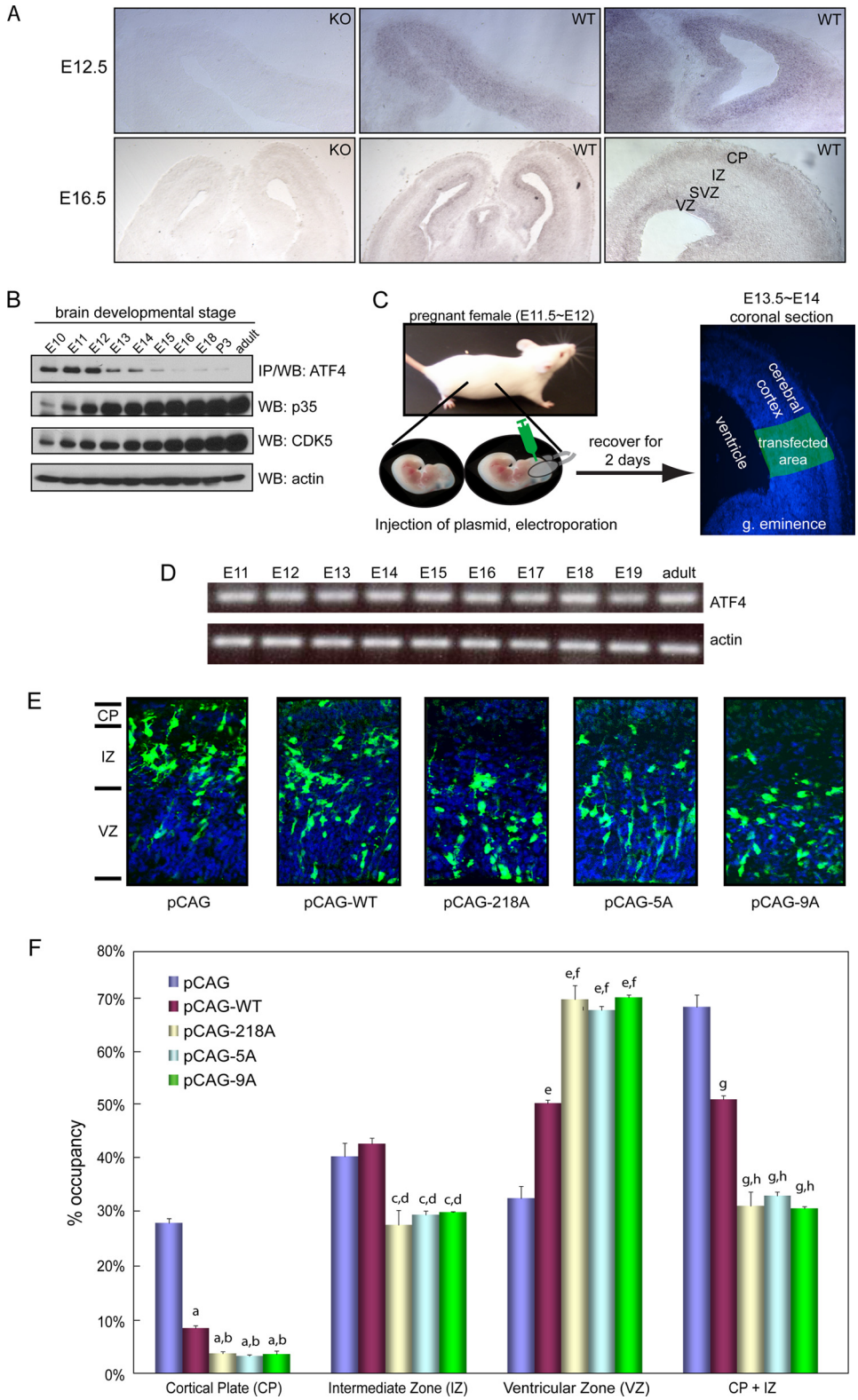

FIGURE 6. **ATF4 degradation is required for proper cell positioning in the developing embryonic brain.** *A*, *in situ* hybridization of wild type and ATF4 knock-out mouse brains from E12.5 and E16.5. *B*, ATF4 was immunoprecipitated from RIPA brain lysates from the indicated ages and subjected to immunoprecipitation and immunoblot analysis with ATF4 antibody. Input lysates were probed with antibodies against p35, CDK5, and actin. *C*, *in utero* electroporation scheme. *D*, RT-PCR analysis of ATF4 and actin brain mRNA from the indicated ages. *E*, brains were electroporated with pCAG, pCAG-WT, pCAG-S218A, pCAG-5A, or pCAG-9A (all proline-directed sites mutated) at E11.5 and fixed 2 days later at E13.5. Brain sections (12 μm) were prepared and stained with an anti-GFP antibody (*green*). Nuclei were stained with Hoechst 33258 (*blue*). *F*, quantification of cell positioning from *D*. Positioning of GFP-positive cells were scored as the percentage of cells in the VZ, IZ, or CP. Data are presented as the mean ± S.E. ($n = 3$). Ventricular zone: *a*, GFP to WT, S218A, 5A, and 9A $p < 0.001$; *b*, WT to S218A, 5A, and 9A, $p < 0.001$. Intermediate zone: *c*, GFP to S218A and 5A, $p < 0.01$, GFP to 9A, $p < 0.001$; *d*, WT to 5A, $p < 0.01$, WT to S218A, 9A, $p < 0.001$. Ventricular zone: *e*, GFP to WT, S218A, 5A, and 9A, $p < 0.001$; *f*, WT to S218A, 5A, and 9A, $p < 0.001$. Intermediate zone + cortical plate: *g*, GFP to WT, S218A, 5A, and 9A, $p < 0.001$; *h*, WT to S218A, 5A, and 9A, $p < 0.001$. *p* values were obtained by one-way analysis of variance.

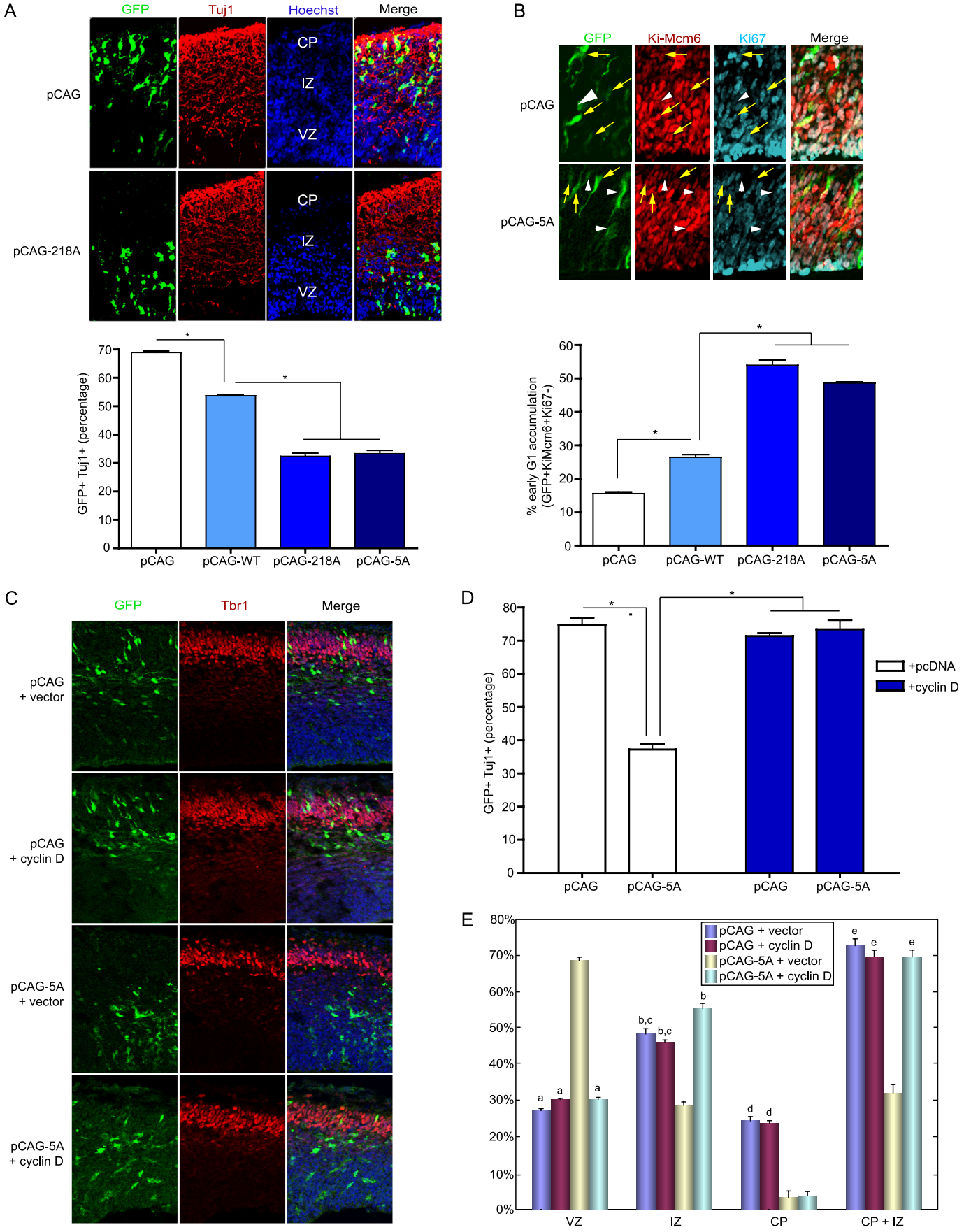
A
GFP
Tuj1
Hoechst
Merge
pCAG
pCAG-218A
CP
IZ
VZ
GFP+ Tuj1+ (percentage)
pCAG
pCAG-WT
pCAG-218A
pCAG-5A
B
GFP
Ki-Mcm6
Ki67
Merge
pCAG
pCAG-5A
% early G1 accumulation (GFP+KiMcm6+Ki67-)
C
GFP
Tbr1
Merge
pCAG + vector
pCAG + cyclin D
pCAG-5A + vector
pCAG-5A + cyclin D
D
+pcDNA
+cyclin D
GFP+ Tuj1+ (percentage)
E
pCAG + vector
pCAG + cyclin D
pCAG-5A + vector
pCAG-5A + cyclin D
VZ
IZ
CP
CP + IZ

expression, we observed a dramatic rescue of neurogenesis in the 5A mutant expressing cells (Fig. 7, *C* and *D*). In contrast, cyclin D only partially rescued cell positioning (Fig. 7, *C* and *E*). Positioning of cells in the IZ increased in cyclin D-coexpressing 5A mutant electroporated brains compared with the GFP control, and correspondingly fewer cells entered the CP. This suggests that proper control of ATF4 is likely also important for coordinating neuronal migration. Collectively, these results demonstrate that neural progenitors arrested in early G_1 by ATF4 stabilization fail to undergo efficient neurogenesis. Importantly, resolving the early G_1 block by co-expressing cyclin D restores differentiation, underscoring the importance of proper G_1 phase control and cell cycle progression for neurogenesis.

DISCUSSION

In this study, we define a novel mechanism whereby multisite phosphorylation regulates ATF4 stability. The requirement for multiple convergent modifications to elicit a single output, degradation, implies that ATF4 dose is kept under tight control. Our study supports this notion by detailing the negative consequences of sustained ATF4 expression. Importantly, we demonstrate a requirement for precise control of ATF4 dose during neurogenesis *in vivo*, a developmentally relevant context.

Multisite Phosphorylation as a Regulatory Mechanism for ATF4 Degradation—ATF4 expression is regulated at the post-transcriptional level (12, 20). ATF4 levels increase under conditions of limited nutrient availability, involving a mechanism of selective reading frame translation. Our findings are not incompatible with such a mechanism. A likely scenario involves a superimposition of the two mechanisms, allowing additional control over a protein whose levels need to be tightly regulated. We speculate that under conditions requiring rapid fluctuations in ATF4 levels, termination of Ser^{218} phosphorylation could confer an acute increase that can be augmented by a more sustained expression offered by increased translation. Furthermore, downstream termination of ATF4 signaling is likely to rely on timely degradation.

The dependence of ATF4 degradation on the F-box protein β-TrCP has been previously described (22, 23), however, the mechanistics of degron phosphorylation were unknown. By providing a detailed picture of the multiple upstream events surrounding degron recognition, our study fills this void and contributes to the notion that ATF4 expression is under multiple layers of control. Both Wnt and Hedgehog signaling are also subject to regulation by β-TrCP, CK1, and GSK3-dependent mechanisms involving β-catenin (30) and *Cubitus interruptus* (31) degradation, respectively. In the case of β-catenin, CK1α acts as a priming kinase. Once primed, GSK3β is recruited and catalyzes consecutive phosphorylation events culminating in degron phosphorylation. With ATF4, however, our results support a more indirect mechanism for degron charging. Single PDP mutants still exhibit considerable degron phosphorylation, a result inconsistent with a priming phosphorylation cascade. Although GSK3β can charge the degron of some β-TrCP substrates, including β-catenin, the ATF4 degron does not conform to its consensus. Interestingly, CK1 seems to function as an opportunistic effector of Ser^{218} phosphorylation. In our model, ATF4 requires no priming phosphorylation, unlike most CK1 substrates, due to the presence of a priming acidic residue, and its recruitment is independent of PDP. CK1 is constitutively active, so what prevents constant charging of the degron? We speculate that the rate-limiting step is the gradual structural unmasking of the degron by multiple phosphorylation events. The degron likely exists in differentially accessible conformation states depending on the particular PDP state. In support of this, mutations most proximal to Ser^{218} have the greatest effect on degron phosphorylation, consistent with localized structure relaxation, whereas distal mutations have correspondingly diminished effects. Another possibility is that each PDP event forms a suboptimal binding interface for a molecule that can influence degron phosphorylation, although this possibility does not take into account the spatial correlations just described. Also important to note is that degron phosphorylation alone is unlikely to be solely responsible for degradation, as the single mutants do not exhibit corresponding effects on stability (Fig. 2*A*) and the degron and 5A mutant interact to some extent with β-TrCP (Fig. 2, *C* and *D*). Additional work will be needed to define the full spectrum of controls that exist to fully execute the ATF4 degradation program.

ATF4 Degradation Is Required for Proper Cell Cycle Control and Neurogenesis—The ability of ATF4 to potently suppress proliferation and elicit G_1 arrest is likely relevant to growth arrest mediated by PERK, an eIF-2α kinase upstream of ATF4 in the unfolded protein response. Activation of the unfolded protein response triggers G_1 arrest that is, in part, dependent on the repression of cyclin D translation (32). A recent report also implicates PERK in limiting the growth of mammary epithelial cells (33). We speculate that ATF4 may bridge a gap between PERK and inhibition of proliferation by providing a transcrip-

FIGURE 7. **Stabilization of ATF4 results induces an early G_1 block in neural progenitors and inhibits neurogenesis *in vivo*.** *A*, embryonic brains (E11.5) were electroporated with pCAG, pCAG-WT, pCAG-S218A, pCAG-5A, fixed 48 h later, and processed for immunohistochemistry. Sections were stained with antibodies against GFP (*green*) and Tuj1 (*red*). Nuclei were stained with Hoechst 33258 (*blue*). A representative image is shown demonstrating that cells remaining in the ventricular zone are negative for Tuj1. Data are presented as the mean ± S.E. ($n = 3$). *, $p < 0.001$ (one-way analysis of variance). *B*, embryonic brains electroporated with the indicated plasmids were analyzed for early G_1 arrest by staining with antibodies against GFP (*green*), Ki-Mcm6 (*red*), and Ki-67 (*light blue*). Shown is the ventricular zone. *Yellow arrows*, early G_1 phase (GFP + Ki-Mcm6 + Ki-67). *White arrowheads*, non-early G_1 cells. Data are presented as mean ± S.E. ($n = 3$). *, $p < 0.001$ (one-way analysis of variance). *C*, E11.5 embryonic brains were electroporated with pCAG or pCAG-5A in combination with cyclin D or a vector control. Processed brains were stained as in *A*, except that Tbr1 antibody was used in place of Tuj1. *D*, quantification of neurogenesis from brain sections of *C* stained with Tuj1 antibody in place of the TBR1 antibody. Data are presented as the mean ± S.E. ($n = 3$). *, $p < 0.001$ (one-way analysis of variance). *E*, quantification of cell positioning from *C*. Data are presented as the mean ± S.E. ($n = 3$). *a,* 5A + vector to pCAG + vector, pCAG + cyclin D, 5A + cyclin D, $p < 0.001$; *b*, 5A + vector to pCAG + vector, pCAG + cyclin D, 5A + cyclin D, $p < 0.001$; *c*, 5A + cyclin D to pCAG + vector and pCAG + cyclin D, $p < 0.01$; *d*, 5A + vector, 5A + cyclin D to pCAG + vector, pCAG + cyclin D, $p < 0.001$; *e*, 5A + vector to pCAG + vector, pCAG + cyclin D, 5A + cyclin D, $p < 0.001$. *p* values were obtained by one-way analysis of variance.

tional component to these responses. In addition, ATF4 may functionally interact with other ATF/CREB family members in transcriptional pathways with downstream consequences on cell cycle progression.

In addition to its degradation, ATF4 expression is also required for cell proliferation (13, 16). ATF4 knock-out embryos display reduced liver hematopoetic progenitor proliferation and ATF4 null mouse embryonic fibroblasts are defective in proliferation. In terms of total brain size, whereas the knock-out mice on average have smaller brains, this phenotype is incompletely penetrant (data not shown). Our observation that ATF4 expression increases in S-phase suggests that, in addition to regulating metabolic genes, ATF4 may target promoters of genes required for cell cycle progression. This dual requirement for expression and degradation may be reflected in its oscillating expression during the cell cycle.

The G_1 phase of the cell cycle is particularly important during embryonic neurogenesis. Increased G_1 length in neural progenitors correlates with increased neurogenesis (34–36), and expressing inhibitors of the G_1/S transition or treating cells with cell cycle inhibitors also promote neurogenesis (37–39). We demonstrate that ATF4-mediated early G_1 arrest potently inhibits neurogenesis. This finding highlights a requirement for proper cell cycle progression for neuronal differentiation. Supporting this hypothesis is our observation that restoring cell cycle progression by coexpression of cyclin D can rescue the neurogenic defect. Our finding that cyclin D can rescue neurogenesis but not cell positioning indicates that ATF4 levels need to be properly controlled in post-mitotic neurons as well, highlighting the importance of temporal regulation of ATF4 levels not only during the cell cycle, but also during development.

Implications of Regulated ATF4 Persistence—Although we delineate a mechanism controlling ATF4 persistence and its relevance in cell cycle progression and brain development, we envision that there are other contexts where precise control of ATF4 dosage is crucial. ATF4 is an important mediator of synaptic plasticity and an inhibitor of CREB, a critical regulator of learning and memory (9, 18, 19, 40). Likewise, control of ATF4 levels, by manipulating the phosphorylation state of the translation initiation factor eIF-2α, can bidirectionally regulate long term potentiation and memory (19). This raises the prospect that phosphorylation-mediated rheostat control of ATF4 persistence might be relevant in this context. It is tempting to speculate that in the basal state, neurons express a steady level of ATF4 controlled by a constant synthetic rate coupled to a permissive degree of degradation. This balance is likely maintained by GCN2 (40) and multiple proline-directed kinases. On demand, inputs from these kinases can be adjusted accordingly to offer neurons a measure of relief from ATF4 and permit fine-tuning of the threshold required to elicit an appropriate degree of CREB-dependent transcription.

A number of questions remain outstanding. Upstream kinases that regulate the specific PDP events will need to be elucidated in future studies. At least in the context of the cell cycle, it is likely that CDKs play a role in this process given the cell cycle-dependent oscillation of ATF4 levels. A thorough analysis of the Ser^{218} kinase is also in order. Although our data provides evidence that CK1 may play a role in this process, more rigorous pursuits will be required to conclusively establish CK1 as a Ser^{218} kinase. Third, although our study focused on the regulation of ATF4 persistence and the impact this has on the cell cycle both *in vitro* and *in vivo*, the underlying defect that contributes to early G_1 arrest has not been elucidated. To this end, further studies directed to examine the transcriptional profile of G_1 genes may provide interesting insights.

In conclusion, we provide a framework for understanding the complexities linking ATF4 phosphorylation and degradation to the regulation of cell cycle progression and neurogenesis. In addition to addressing a biologically relevant question, deciphering the subtleties that surround the control of ATF4 stability and its effect on suppressing proliferation and neurogenesis holds therapeutic potential in putting a break on the runaway growth of cancer cells and manipulating the production of neurons.

Acknowledgments—We thank B. Samuels, D. Kim, X. Ang, J. Buchman, and J. Hsu for critical reading of the manuscript. We thank Dr. Wade Harper for β-TrCP and CK1 related constructs, Dr. Sander van den Huevel for the cyclin D1 construct, and Drs. Osamu Tetsu and Frank McCormick for the cyclin D1 promoter constructs. We are also grateful to Dr. Jeff Leiden (via Dr. Laurie Glimcher) for providing the ATF4 knock-out mice.

REFERENCES

1. Jackson, P. K., and Eldridge, A. G. (2002) *Mol. Cell* **9,** 923–925
2. Cardozo, T., and Pagano, M. (2004) *Nat. Rev. Mol. Cell Biol.* **5,** 739–751
3. Ang, X. L., and Harper, W. J. (2005) *Oncogene* **24,** 2860–2870
4. Reed, S. I. (2003) *Nat. Rev. Mol. Cell Biol.* **4,** 855–864
5. Nakayama, K. I., and Nakayama, K. (2006) *Nat. Rev. Cancer* **6,** 369–381
6. Nash, P., Tang, X., Orlicky, S., Chen, Q., Gertler, F. B., Mendenhall, M. D., Sicheri, F., Pawson, T., and Tyers, M. (2001) *Nature* **414,** 514–521
7. Pufall, M. A., Lee, G. M., Nelson, M. L., Kang, H. S., Velyvis, A., Kay, L. E., McIntosh, L. P., and Graves, B. J. (2005) *Science* **309,** 142–145
8. Strickfaden, S. C., Winters, M. J., Ben-Ari, G., Lamson, R. E., Tyers, M., and Pryciak, P. M. (2007) *Cell* **128,** 519–531
9. Chen, A., Muzzio, I. A., Malleret, G., Bartsch, D., Verbitsky, M., Pavlidis, P., Yonan, A. L., Vronskaya, S., Grody, M. B., Cepeda, I., Gilliam, T. C., and Kandel, E. R. (2003) *Neuron* **39,** 655–669
10. Sanada, K., and Tsai, L. H. (2005) *Cell* **122,** 119–131
11. Shu, T., Tseng, H. C., Sapir, T., Stern, P., Zhou, Y., Sanada, K., Fischer, A., Coquelle, F. M., Reiner, O., and Tsai, L. H. (2006) *Neuron* **49,** 25–39
12. Harding, H. P., Novoa, I., Zhang, Y., Zeng, H., Wek, R., Schapira, M., and Ron, D. (2000) *Mol. Cell* **6,** 1099–1108
13. Harding, H. P., Zhang, Y., Zeng, H., Novoa, I., Lu, P. D., Calfon, M., Sadri, N., Yun, C., Popko, B., Paules, R., Stojdl, D. F., Bell, J. C., Hettmann, T., Leiden, J. M., and Ron, D. (2003) *Mol. Cell* **11,** 619–633
14. Tanaka, T., Tsujimura, T., Takeda, K., Sugihara, A., Maekawa, A., Terada, N., Yoshida, N., and Akira, S. (1998) *Genes Cells* **3,** 801–810
15. Hettmann, T., Barton, K., and Leiden, J. M. (2000) *Dev. Biol.* **222,** 110–123
16. Masuoka, H. C., and Townes, T. M. (2002) *Blood* **99,** 736–745
17. Yang, X., Matsuda, K., Bialek, P., Jacquot, S., Masuoka, H. C., Schinke, T., Li, L., Brancorsini, S., Sassone-Corsi, P., Townes, T. M., Hanauer, A., and Karsenty, G. (2004) *Cell* **117,** 387–398
18. Bartsch, D., Ghirardi, M., Skehel, P. A., Karl, K. A., Herder, S. P., Chen, M., Bailey, C. H., and Kandel, E. R. (1995) *Cell* **83,** 979–992
19. Costa-Mattioli, M., Gobert, D., Stern, E., Gamache, K., Colina, R., Cuello, C., Sossin, W., Kaufman, R., Pelletier, J., Rosenblum, K., Krnjević, K., Lacaille, J. C., Nader, K., and Sonenberg, N. (2007) *Cell* **129,** 195–206
20. Lu, P. D., Harding, H. P., and Ron, D. (2004) *J. Cell Biol.* **167,** 27–33
21. Xie, Z., Moy, L. Y., Sanada, K., Zhou, Y., Buchman, J. J., and Tsai, L. H.

(2007) *Neuron* **56,** 79–93
22. Lassot, I., Ségéral, E., Berlioz-Torrent, C., Durand, H., Groussin, L., Hai, T., Benarous, R., and Margottin-Goguet, F. (2001) *Mol. Cell. Biol.* **21,** 2192–2202
23. Yang, X., and Karsenty, G. (2004) *J. Biol. Chem.* **279,** 47109–47114
24. Heidebrecht, H. J., Buck, F., Endl, E., Kruse, M. L., Adam-Klages, S., Andersen, K., Frahm, S. O., Schulte, C., Wacker, H. H., and Parwaresch, R. (2001) *Lab. Invest.* **81,** 1163–1165
25. Yukawa, K., Tanaka, T., Tsuji, S., and Akira, S. (1999) *Brain Res. Mol. Brain Res.* **69,** 124–134
26. Nehring, R. B., Horikawa, H. P., El Far, O., Kneussel, M., Brandstätter, J. H., Stamm, S., Wischmeyer, E., Betz, H., and Karschin, A. (2000) *J. Biol. Chem.* **275,** 35185–35191
27. White, J. H., McIllhinney, R. A., Wise, A., Ciruela, F., Chan, W. Y., Emson, P. C., Billinton, A., and Marshall, F. H. (2000) *Proc. Natl. Acad. Sci. U.S.A.* **97,** 13967–13972
28. Vernon, E., Meyer, G., Pickard, L., Dev, K., Molnar, E., Collingridge, G. L., and Henley, J. M. (2001) *Mol. Cell. Neurosci.* **17,** 637–645
29. Ritter, B., Zschüntsch, J., Kvachnina, E., Zhang, W., and Ponimaskin, E. G. (2004) *Brain Res. Dev. Brain Res.* **149,** 73–77
30. Liu, C., Li, Y., Semenov, M., Han, C., Baeg, G. H., Tan, Y., Zhang, Z., Lin, X., and He, X. (2002) *Cell* **108,** 837–847
31. Price, M. A., and Kalderon, D. (2002) *Cell* **108,** 823–835
32. Brewer, J. W., and Diehl, J. A. (2000) *Proc. Natl. Acad. Sci. U.S.A.* **97,** 12625–12630
33. Sequeira, S. J., Ranganathan, A. C., Adam, A. P., Iglesias, B. V., Farias, E. F., and Aguirre-Ghiso, J. A. (2007) *PLoS ONE* **2,** e615
34. Miyama, S., Takahashi, T., Nowakowski, R. S., and Caviness, V. S., Jr. (1997) *Cereb. Cortex* **7,** 678–689
35. Götz, M., and Huttner, W. B. (2005) *Nat. Rev. Mol. Cell Biol.* **6,** 777–788
36. Frank, C. L., and Tsai, L. H. (2009) *Neuron* **62,** 312–326
37. Mitsuhashi, T., Aoki, Y., Eksioglu, Y. Z., Takahashi, T., Bhide, P. G., Reeves, S. A., and Caviness, V. S., Jr. (2001) *Proc. Natl. Acad. Sci. U.S.A.* **98,** 6435–6440
38. Calegari, F., and Huttner, W. B. (2003) *J. Cell Sci.* **116,** 4947–4955
39. Tarui, T., Takahashi, T., Nowakowski, R. S., Hayes, N. L., Bhide, P. G., and Caviness, V. S. (2005) *Cereb. Cortex* **15,** 1343–1355
40. Costa-Mattioli, M., Gobert, D., Harding, H., Herdy, B., Azzi, M., Bruno, M., Bidinosti, M., Ben Mamou, C., Marcinkiewicz, E., Yoshida, M., Imataka, H., Cuello, A. C., Seidah, N., Sossin, W., Lacaille, J. C., Ron, D., Nader, K., and Sonenberg, N. (2005) *Nature* **436,** 1166–1173
41. Tetsu, O., and McCormick, F. (1999) *Nature* **398,** 422–426